





Structural correlation and chemistry of molten NaF–ScF₃ with dissolved metal aluminium: TG/DTA, XRD, NMR and molecular dynamics simulations

Aydar Rakhmatullin* , František Šimko* , Didier Zanghi, Zuzana Netriová, Ilya B. Polovov, Ayrat Dimiev, Konstantin V. Maksimtsev, Catherine Bessada, Michal Korenko

Received: 29 May 2023 / Revised: 3 November 2023 / Accepted: 5 November 2023 / Published online: 25 April 2024
© The Author(s) 2024

Abstract For the first time, the mechanism of metal aluminium dissolution in NaF–ScF₃ eutectic melts and the chemical interaction between the constituents of this mixture have been thoroughly studied by a combination of differential thermal analysis (DTA), high temperature and solid-state nuclear magnetic resonance (NMR), and X-ray diffraction (XRD) coupled with the molecular dynamic simulations. The formation of an insoluble Al₃Sc alloy in molten (NaF–ScF₃)_{eut} system was proven, and the chemical mechanism of this aluminothermic Al₃Sc alloy production was elucidated. Corresponding ex situ examinations bring to light the formation of

NaScF₄ and solid solution of Na₃(Al,Sc)F₆ in cooled bath. The molecular dynamics calculations of the bath allow us to construct the structural model and to predict viscosity, density and electrical conductivity of the reagent melt to help to optimize the conditions of the alloy synthesis.

Keywords Scandium; Alloy; Molten salts; NMR; Molecular dynamics

Supplementary Information The online version contains supplementary material available at <https://doi.org/10.1007/s12598-024-02690-0>.

A. Rakhmatullin*, D. Zanghi, C. Bessada
Conditions Extrêmes et Matériaux: Haute Température et Irradiation, CEMHTI, UPR 3079 -CNRS Univ Orleans, 45071 Orléans, France
e-mail: rakhmat@cnrs-orleans.fr

F. Šimko*, Z. Netriová, M. Korenko
Department of Molten Systems, Institute of Inorganic Chemistry, Slovak Academy of Sciences, 845 36 Bratislava, Slovakia
e-mail: uachsim@savba.sk

F. Šimko, M. Korenko
Centre of Excellence for Advanced Materials Application - CEMEA, Slovak Academy of Sciences, 845 11 Bratislava, Slovakia

I. B. Polovov, K. V. Maksimtsev
Department of Rare Metals and Nanomaterials, Institute of Physics and Technology, Ural Federal University, 620002 Ekaterinburg, Russia

A. Dimiev
Alexander Butlerov Institute of Chemistry, Kazan Federal University, 420008 Kazan, Russia

Introduction

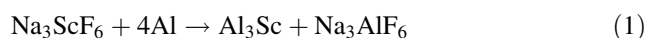
It is well established that tiny infusion of a rare earth metal scandium to aluminum alloys radically improves the tensile strength and desirable physical properties of the alloy product. Scandium strengthens aluminum products in three distinct paths: grain refining, precipitation hardening and preventing recrystallization or diminishing grain growth. Scandium raises the recrystallization temperature of aluminum alloys to further aloft 600 °C, which is well enough for the heat-treatable aluminum alloys. Using small scandium concentrations, between 0.1 wt% and 0.45 wt%, yields the excellent strength characteristics by a smaller, even-sized grain structure in alloys during the solidification process (50–100 MPa increment of strength per 0.1 wt% Sc added) [1].

Currently, the establishment of economically profitable conditions for producing scandium is a relevant task, because the requisition for high-purity scandium raw materials, above all in the aerospace industry, whether it is oxide or fluoride, is progressively growing. Meanwhile, the high cost of scandium hinders commissioning its large-scale production.

The greatest contribution to the cost of scandium products has come from the leaching of scandium from ore or waste [2–4]. Scandium content in processing products of



raw material amounts to 1–10 parts per million (ppm, $\times 10^{-6}$). Once initial concentrates are obtained, these are further processed into scandium compounds. Thus, the cost of final products can be reduced via the synthesis of principal metal or raw materials, combined by the production of scandium. For example, the raw materials can be uranium-leaching solutions or hydrolytic acid, released upon the titanium dioxide fabrication. Very recently, a new original technological process based on the recovery of scandium from uranium ores was developed and put into practice [5]. The final product was scandium concentrate based on NaScF₄ [6]. The main advantage of this method is the ability to use directly as obtained scandium concentrate without additional purification in order to obtain an Al–Sc alloy by adding aluminum metal into molten concentrate. The reduction of Sc by aluminum from Na₃ScF₆ proceeds according to the below reaction:



Therefore, the investigation of the reaction of scandium fluoride with metallic aluminum directly in the molten bath is a relevant task from the fundamental and as well as industrial point of view with the main aim to understand the mechanism of the Al₃Sc formation.

In our previous paper, the local structure of scandium and fluoride ions in the molten NaF–ScF₃ system within a wide range of composition (from 0 to 70 mol% of ScF₃) has been established. An average coordination number of 6 had been determined for scandium in all domains of its composition, and the formation of a network structure in the melt was shown as well [7].

The present work aims the laboratory study relying on the combination of high temperature (HT) and solid-state nuclear magnetic resonance (NMR), X-ray diffraction (XRD) and differential thermal analysis (DTA) of the molten mixtures whose compositions are identical to those used for the production of intermetallic Al₃Sc, i.e., (NaF–ScF₃)_{eut} + Al or 63 mol% NaF–37 mol% ScF₃ + Al. The experimental study is also supported by the molecular dynamic simulations. A molecular dynamics simulation study of the molten NaF–ScF₃–AlF₃ system was performed to further understand the local and global structure of the molten reaction mixture and to find the match between this structure of the melt and its possible physicochemical behavior (density, viscosity, electrical conductivity, etc.).

Experimental

Materials

For the preparation of the samples, the following chemicals were used: sodium fluoride (NaF, CAS Number: 7681-49-

4), Sigma-Aldrich, ACS reagent $\geq 99\%$, dried in vacuum at 773 K for 4 h; scandium fluoride (ScF₃, CAS number: 13709-47-2), JSC Dalur $> 99\%$; aluminum powder (Al, CAS number: 7429-90-5), Alfa Aesar, – 325 mesh, 99.5% (metals basis).

All chemicals were stored in a glove box under argon atmosphere (Ar, SIAD, 99.999%) maintained below 0.3×10^{-6} of moisture and 0.1×10^{-6} – 0.5×10^{-6} of oxygen.

Samples preparation

The samples, analyzed at room temperature using X-ray and solid-state NMR analysis, were prepared in glove box. The compositions of (NaF–ScF₃)_{eut} were prepared by mixing and grinding the corresponding fluorides. Individual mixtures with different amount of aluminum (100 mg) were weighted into the boron nitride crucibles with lid (boron nitride (BN, CAS Number: 10043-11-5), P Vision-ABC France, 99.99%, Crucible $\Phi 9$, hole $\Phi 2.5 \times 7$ mm deep), closed and sealed into the capsule. Samples were en bloc heated in a resistance furnace under an atmosphere of dried argon (Messer, 99.996% purity) from room temperature up to 680 °C at a heating rate of $5 \text{ °C} \cdot \text{min}^{-1}$ under 0.3 MPa of argon atmosphere. The holding time was 100 min. The temperature control and the data processing were performed using a computerized measuring device (multicomponent model for thermal analysis data collections National Instruments, where the data collections run online under LabVIEW software). The temperature of the samples was controlled by a Pt–PtRh10 thermocouple, calibrated on the melting points of highly pure NaCl and NaF (sodium chloride ultrapure (NaCl, CAS number: 7647-14-5) 99.9%, powder and sodium fluoride (NaF, CAS number: 7681-49-4) 99.9%, powder; both Alfa Aesar by Thermo Fischer Scientific GmbH, Germany). The accuracy of the temperature difference measurement between the temperatures of primary crystallizations of the given mixtures was ($\pm 1 \text{ °C}$). After melting, the samples were then spontaneously cooled down to room temperature at a rate of $7 \text{ °C} \cdot \text{min}^{-1}$. The samples were then homogenized in glove box and ready for analysis by MAS NMR and XRD.

TG/DTA analysis

The thermal properties of the basic mixture (NaF–ScF₃)_{eut} with different amount of Al were investigated by means of differential scanning calorimetry performed with a NETZSCH simultaneous thermal analyzer STA 449 F3 Jupiter®. All samples (60 mg) were individually weighted in a glove box under inert atmosphere (Ar, Messer, 99.999% purity) and placed in a sintered Al₂O₃ (99.7%) crucible and closed in an simultaneous thermal analysis

(STA) apparatus. The system was one time evacuated and then measured under an argon (Ar, 99.999%) atmosphere (50 mL·min⁻¹). Phase transition data were obtained from heating and cooling curves. Every sample was heated at 7 °C·min⁻¹ up to 50 °C above the liquidus temperature and subsequently cooled to ambient temperature by a cooling rate of 1.4 °C·min⁻¹. A baseline correction measurement for the empty crucible was done under the same conditions as the sample measurements. Calibration of temperature and sensitivity ($\pm 3\%$) was done for the pure Al. The NETZSCH Proteus Thermal Analysis software was used for data processing and for evaluation of the experimental thermogram. The X-ray technique was used for identification of new phases in the measured system.

Powder XRD

Powder XRD patterns of all the spontaneously cooled samples were measured using an Empyrean PANalytical diffractometer with Cu K $\alpha_{1,2}$ radiation in Bragg–Brentano geometry and a β filter (Ni). A solid-state PIXcel detector was used to record XRD patterns. The measurements were taken at room temperature, with 2θ varying from 5° to 80° at a step of 0.0261°. The time per step was 26 s. Phase analysis was performed with Oxford Cryosystem Crystallographica Search-Match 2.1 software with PDF2 2011 database.

NMR spectroscopy

The HT NMR setup was identical to our previous work, and the study was carried out on a Bruker Avance 400 spectrometer. A single-pulse sequence was used for high-temperature experiments with the pulse widths of 19.5 μ s for ¹⁹F and 27.5 μ s for ⁴⁵Sc and ²⁷Al corresponding to a nutation frequency ω_1 of 12.8 and 9.1 kHz. In all ²⁷Al and ⁴⁵Sc NMR measurements, the spectral width 200 kHz is larger than excitation bandwidth. To avoid this problem and do not lose signal, we recorded three spectra for each composition with the same parameters but with different offset: one at around 0, one at metal signal and one in the middle between the two previous cases.

Solid-state MAS NMR spectra were measured at 20 T using a Bruker AVANCE III HD spectrometer with 1.3-mm probe. Very short 0.2 μ s ($\approx \pi/12$ and $\omega_1 = 1.25$ MHz) pulses were used for ²⁷Al and ⁴⁵Sc to excite the full spectral width (750 kHz and 1.15 MHz for ²⁷Al and ⁴⁵Sc) with a single scan. The ¹⁹F pulse length was of 0.71 μ s ($\pi/2$). The recycle delays were 120 s (¹⁹F) and 0.5 s (²⁷Al and ⁴⁵Sc). All MAS NMR spectra were acquired at a spinning frequency of 60 kHz, and the number of scans was enough to acquire a good signal-to-noise ratio. PISSARRO [8] decoupling pulse sequence was used to increase the

Table 1 Pair potential parameters used in polarizable ion model

Ion pair	B_{ij}	α_{ij}	C_{ij}^6	C_{ij}^8
Sc ³⁺ –Al ³⁺	1.13	13.10	59.52	799.85

resolution of the ⁴⁵Sc and ¹⁹F spectra. The ¹⁹F, ²³Na, ²⁷Al and ⁴⁵Sc spectra were referenced to the external standards of CFCl₃, 1 mol·L⁻¹ NaCl, 1 mol·L⁻¹ Al(NO₃)₃ and 0.11 mol·L⁻¹ ScCl₃, respectively.

Computational details

The same approach and methodology was applied as in our previous works for NaF–AlF₃ and NaF–ScF₃ systems [7, 9].

The parameters of new potential Sc³⁺–Al³⁺ were obtained according to the procedure described in previous works [7, 9] and are presented in Table 1. Pair potential parameters are used in the polarizable ion model (all of the parameters are given in atomic unit (au)), where B_{ij} and α_{ij} are parameters from the repulsion term; C_{ij}^6 and C_{ij}^8 are, respectively, dipole–dipole and dipole–quadrupole terms from the dispersion component between two ions at a longer range.

Results and discussion

Thermal analysis

The phase equilibria of the eutectic system NaF–ScF₃ (63 mol% NaF–37 mol% ScF₃) with different addition amounts of aluminum (up to max. 80 mol%) are presented in Fig. 1. TG/DTA study was performed to determine the solubility of aluminum in the eutectic system of NaF–ScF₃. After several heating–cooling cycles, the thermogravimetry of the samples also showed a mass loss of around 0.2–0.5 wt%. These very low losses indicate the stability of the system in this temperature range.

TG/DTA shows the presence of two or three peaks, depending on the amount of aluminum added. For the (NaF–ScF₃)_{eut} sample without aluminum, two peaks located at 658 and 648 °C were observed. These values are in accordance with those reported in phase diagram established by Thoma and Karraker [10]. According to these data, a first transition around 660 °C was observed during the cooling. This temperature corresponds to the transition from a liquid state to a mixture composed of liquid and solid NaScF₄. A second transition, obtained at 650 °C, is related to the transition from the above-mentioned state to a solid solution of NaScF₄ and Na₃ScF₆.

As it can be seen from Fig. 1, the temperature of the thermal effects in our systems varies with the aluminum

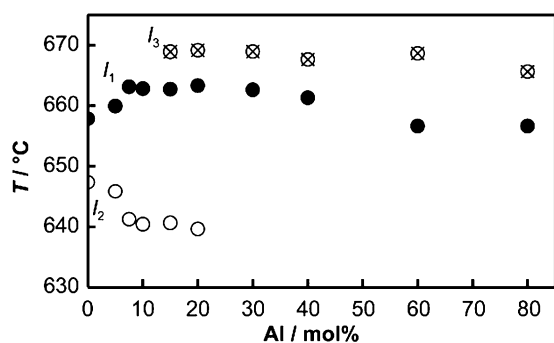


Fig. 1 DTA peak temperatures of system (NaF–ScF₃)_{eut}–Al as a function of aluminum concentration. I_{1-3} : different peaks recorded by DTA

content in the samples. In the case of peak I_1 , the temperature increases in the concentration range of aluminum from 0 to 10 mol%. The peak I_2 has, however, in this concentration range, an opposite trend. The temperature in this case decreases with an increase of the content of aluminum. Since on 10 mol% of Al, the transition temperature related to both peaks (I_1 , I_2) is being stabilized on a plateau value of around 665 and 640 °C, respectively. The second peak disappears at the concentration of aluminum around 20 mol% to be “replaced” by a third peak (I_3) from 15 mol%. The temperature of this peak in the concentration range till 60 mol% of Al oscillates around a value of 670 °C. For the highest Al content, the temperature of the peak I_3 decreases slightly to a value around 665 °C. The similar temperature’s drop in higher concentration of aluminum can also be seen in the case of peak I_1 .

The highest thermal effect (I_3) in Fig. 1 can be explained by a transition between a liquid mixture and Al₃Sc and a solid solution consisting of α -Al and Al₃Sc. According to the Al–Sc phase diagram [11, 12], the transition temperature of the Al–Sc mixture decreases with increasing concentration of aluminum (since on 60 mol% of Al). This observation could therefore also explain the drop of the temperature of the third peak (I_3); we have detected since on 50 mol% of Al. The two peaks (I_1 and I_3) measured by DTA in the sample with 80 mol% of Al (658 and 665 °C, respectively), would therefore be the signature of the transition from the liquid to a mixture of liquid and α -Al and then from this mixture to a solid solution α -Al + Al₃Sc (Fig. 1).

XRD and solid-state MAS NMR analysis of solidified samples

In order to understand the origin of endothermic peaks and their evolution as a function of the concentration of aluminum in (NaF–ScF₃)_{eut} system, XRD and solid-state MAS NMR analysis of the solidified samples were performed.

Figure 2a shows the results of XRD analysis; the MAS NMR analysis can be found in Figs. 3–5.

The X-ray analysis of the solidified samples without aluminum (mixture (NaF–ScF₃)_{eut}) shows the presence of only two compounds (pattern 0 mol% in Fig. 2): the cryolite-like phase, Na₃ScF₆ and NaScF₄. The presence of these compounds is in accordance with the phase diagram reported by Thoma and Karraker [10].

Besides the already observed patterns of NaScF₄ and Na₃ScF₆, XRD patterns of all the mixtures with the aluminum contain the new patterns of two new compounds: Al₃Sc and ScOF. The presence of the oxygen-contained species in the pattern (ScOF) is probably due to a contamination from the hot-pressed boron nitride crucibles. Figure 2 also shows that the intensity of the Al₃Sc diffractions linearly grows with increasing concentration of aluminum in the samples.

The diffractions of Na₃ScF₆ are observed in the whole concentration range of aluminum in the mixtures, and their intensities decrease with increasing concentration of aluminum. Besides that, an interesting change of the shape of these diffractions with the increased concentration of aluminum was observed (Fig. 2b). This change suggests that the compositional variation of the aluminum concentration affects the unit cell parameters as well as the composition of the phase.

The compound Na₃ScF₆ (ICSD No. 401761 [13]) bears a marked crystal symmetry resemblance to Na₃AlF₆ (ICSD No. 4029 [16]), resulting to some sort of X-ray pattern similarity, as it can be seen in Fig. 2b. It can be inferred that the changes of the X-ray patterns of the Na₃ScF₆ observed with the increasing concentration of aluminum in the samples are caused by the formation of a solid solution, where the Sc³⁺ ions in the Na₃ScF₆ structure are being replaced by smaller Al³⁺ ions. This replacement leads necessarily to a modification of the unit cell of Na₃ScF₆, due to a change of the distance between individual lattice sites. The effect of the formation of the fore-mentioned solid solutions is more pronounced at the higher aluminum content (30 mol%–70 mol%), where the continually increasing peak of Na₃AlF₆ (Fig. 2b) can be seen.

The intensity of the signals of the NaScF₄ gradually decreases from 11 mol% of aluminum to complete disappearance above 30 mol%–50 mol%. On the other hand, new diffractions begin to appear in the records at this concentration range. Also, the formation of ScF₃, observed in the X-ray patterns taken on the samples with the higher concentration of aluminum, is very likely a side product of the disappearance of NaScF₄.

All the aluminum containing samples, practically from the very beginning, show the presence of the Al₃Sc alloy in the X-ray patterns. The intensity of the Al₃Sc alloy signal tends to increase with the increase of the aluminum

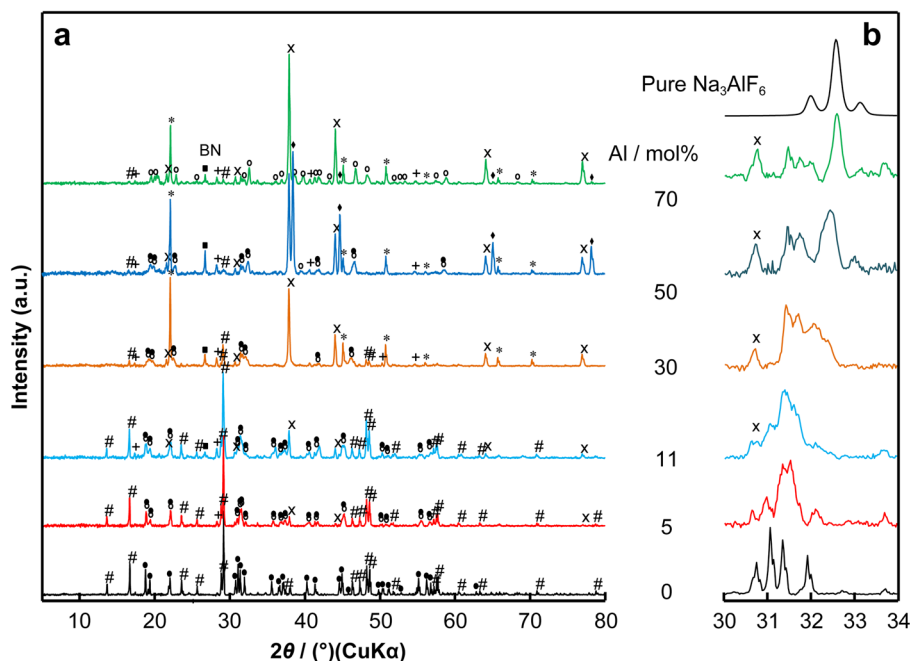


Fig. 2 **a** XRD patterns of solidified samples of $(\text{NaF}-\text{ScF}_3)_{\text{eut}}$ with different amounts of aluminum (from 0 to 70 mol%), **b** selected enlarged region of XRD patterns; #— NaScF_4 [10], ●— Na_3ScF_6 [13], X— Al_3Sc [14], + — ScOF [15], ○— Na_3AlF_6 [16], ○●— $\text{Na}_3(\text{Al,Sc})\text{F}_6$, *— ScF_3 [17], ◆— Al [18]

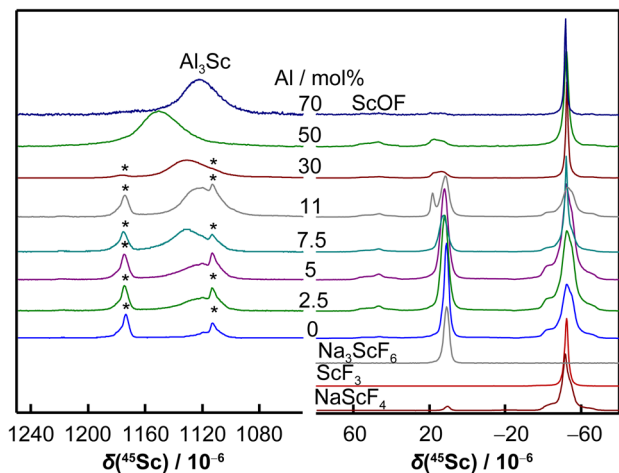


Fig. 3 ^{45}Sc MAS NMR spectra at 20 T of solidified $(\text{NaF}-\text{ScF}_3)_{\text{eut}}$ with 0, 2.5 mol%, 5 mol%, 7.5 mol%, 11 mol%, 30 mol%, 50 mol% and 70 mol% Al, where * represents spinning side bands

concentration. This trend however reaches a plateau at the concentration of 40 mol%. At these very high concentrations, diffraction peaks corresponding to the metallic aluminum also evolved.

To elucidate in more detail the chemistry and the phases presented in the investigated solidified systems, a MAS NMR experiment was carried out to probe the local environment around the ^{27}Al , ^{45}Sc and ^{19}F nuclei. Figure 3 shows ^{45}Sc MAS NMR spectra of the solidified samples of

$\text{NaF}-\text{ScF}_3$ with an addition of different amounts of aluminum (0 to 70 mol% of Al). Figures 4, 5 show spectra of ^{19}F and ^{27}Al , respectively.

At low Al contents, the two main quadrupolar resonance lines in Fig. 3 located around -50×10^{-6} and 10×10^{-6} indicate the presence of NaScF_4 and Na_3ScF_6 compounds, respectively. These findings are in accordance with ^{19}F NMR spectra (Fig. 4). ^{19}F NMR spectra of the mixture with Al content up to 30 mol% contain two sets of signals corresponding to the NaScF_4 , Na_3ScF_6 and one line to Na_3AlF_6 . It is worth to note that there is a broadening of the ^{19}F NMR signals of Na_3ScF_6 and Na_3AlF_6 , which is the result of the decreasing symmetry around fluorine nuclei due to the substitution of Sc by Al atoms, i.e., the result of the formation of solid solutions (the same phenomenon was identified by XRD). The ^{19}F line of Na_3ScF_6 is not resolved, the line width (full width at half-maximum, FWHM) of Na_3AlF_6 increases from 1500 Hz (pure compound) to 2400 Hz. ^{45}Sc spectra more clearly show the formation of a solid solution. The initial resonance of Na_3ScF_6 begins to broaden with increasing aluminum content, and at 11 mol% of Al, a new peak with a symmetric line shape appears at -17.5×10^{-6} . At low Al contents, the solid solutions are not easy to be detected by XRD. This is the reason why in this particular case the NMR is more accurate compared to XRD.

On the other hand, the presence of ScF_3 is difficult to be identified by NMR due to the overlapping with NaScF_4

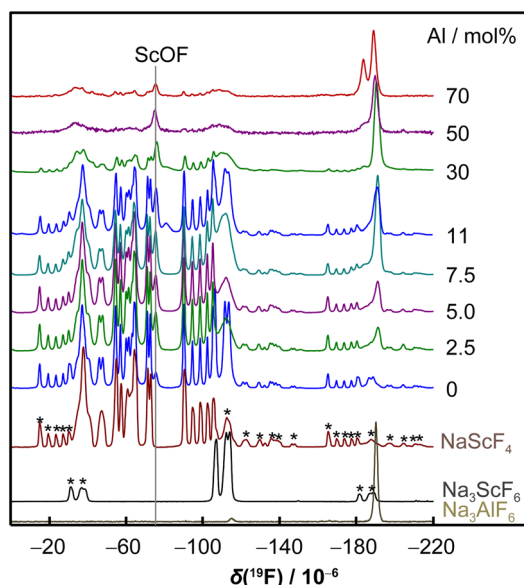


Fig. 4 ^{19}F MAS NMR spectra at 20 T of solidified $(\text{NaF}-\text{ScF}_3)_{\text{eut}}$ with 0, 2.5 mol%, 5 mol%, 7.5 mol%, 11 mol%, 30 mol%, 50 mol% and 70 mol% Al, where * represents spinning side bands; spectra of pure Na_3AlF_6 , Na_3ScF_6 and NaScF_4 were added for the sake of clarity

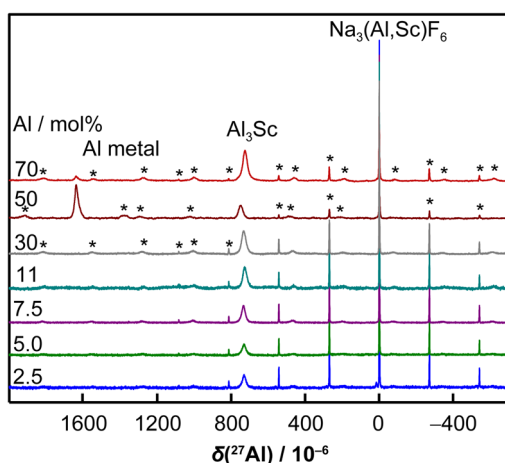


Fig. 5 ^{27}Al MAS NMR spectra at 20 T of solidified $(\text{NaF}-\text{ScF}_3)_{\text{eut}}$ with 0, 2.5 mol%, 5 mol%, 7.5 mol%, 11 mol%, 30 mol%, 50 mol% and 70 mol% Al, where * represents spinning side bands

peaks in both ^{45}Sc and ^{19}F spectra. The presence of Al_3Sc alloy is characterized by a ^{45}Sc peak around 1130×10^{-6} , and it confirms its formation as soon as a few mol% of aluminum is introduced to the $\text{NaF}-\text{ScF}_3$ mixture. The appearance of a small peak with quadrupolar line shape ($\delta_{\text{iso}} = 58.4 \times 10^{-6}$, $C_Q = 12.2$ MHz, $\eta_Q = 0.81$) in ^{45}Sc and with Gaussian line shape ($\delta_{\text{iso}} = -75.6 \times 10^{-6}$) in ^{19}F spectra also confirms the presence of ScOF , where δ_{iso} is isotropic chemical shift, C_Q is quadrupole coupling constant, and η_Q is asymmetry parameter of the

quadrupolar interaction [19]. For the high Al contents of 50% and 70%, one unassigned resonance at -181×10^{-6} can be observed.

^{27}Al MAS NMR spectra (Fig. 5) confirm that for the contents less than 30 mol% of Al, only the resonance lines of AlF_6 octahedra in $\text{Na}_3(\text{Al},\text{Sc})\text{F}_6$ ($\delta_{\text{iso}} = -1.6 \times 10^{-6}$) and in Al_3Sc ($\delta_{\text{iso}} = 728 \times 10^{-6}$) are detected. The intensity of the Al_3Sc peak in ^{27}Al and ^{45}Sc NMR spectra increases with increasing Al content up to 30 mol%. The measured ^{45}Sc and ^{27}Al chemical shifts of Al_3Sc slightly differ from those given by Bastow et al. [20], which is 1100×10^{-6} and 756×10^{-6} , respectively. This difference of the chemical shifts can be explained by the formation of off-stoichiometric compound(s) $\text{Al}_{3-x}\text{Sc}_{1+x}$ [21], where the structural environments around both nuclei are slightly different. Microstructural observations also indicate that the Al_3Sc phase also has a solubility range (immiscibility region where molten Al is in equilibrium with the melt). The characteristic resonance line of Al metal located around 1636×10^{-6} [22, 23] only appears for the concentrations above 30 mol% of Al.

^{23}Na NMR spectra (Fig. S2 in Supporting Information) agree well with the above-mentioned results obtained for other nuclei. Only a spectral signature of the compounds NaScF_4 and Na_3ScF_6 is observed in a sample without Al. The intensity of an envelope of signals of NaScF_4 decreases with increasing Al content. It was already mentioned that the compounds Na_3ScF_6 and Na_3AlF_6 are isostructural [13, 16]. The environment of the two sodium sites in Na_3ScF_6 and Na_3AlF_6 is very similar, and consequently, the shape and the position of the two peaks are very close. With increasing of Al content in the system, the right peak remains almost unchanged, while the left one slowly migrates from the “ Na_3ScF_6 ” position (ca -2×10^{-6}) toward “ Na_3AlF_6 ” one (ca 2.5×10^{-6}). Same as for ^{19}F , for the high Al content of 50%, one unassigned resonance at around -6×10^{-6} can be detected.

It can be mentioned here that both techniques, XRD and solid-state MAS NMR, are useful complement to each other, and our study showed that the obtained results were in good agreement. To see how the in situ evolution of the internal structural environment of the investigated systems in molten state as a function of the aluminum content, a high-temperature (HT) NMR analysis of the ^{27}Al , ^{45}Sc , ^{23}Na and ^{19}F nuclei was also performed. The results of that analysis are presented in the following sub-chapter.

HT NMR in melts

Figure 6 shows HT NMR analysis of the ^{45}Sc nucleus taken at 770 °C in $(\text{NaF}-\text{ScF}_3)_{\text{eut}}-\text{Al}$ mixture. As it can be seen, HT NMR ^{45}Sc spectra of the samples with higher

content of aluminum (59 mol%) have two lines: one narrow corresponding to scandium in liquid melt at -6.7×10^{-6} and the second one, a broad line at 1338×10^{-6} , which is a characteristic line for the solid state. A small drift of the “liquid” line of ^{45}Sc nuclei from -6.7×10^{-6} to 5.5×10^{-6} can be attributed to a slight change in scandium environment in the melt with the increasing content of aluminum (from 11 mol% to 70 mol%). The average coordination number around scandium in the melt is constantly six over the whole range of compositions of Al [24, 25].

The chemical shift of the “solid” line of the system with 70 mol% of Al detected in our work at 770 °C (1338×10^{-6}) is in good agreement with what was reported in Ref. [20]. The authors in this work studied the variation of the ^{45}Sc Knight shift with temperature in Al_3Sc (from room temperature to 960 °C). A strong ^{45}Sc Knight shift dependence on temperature was observed: $\delta = 1100 \times 10^{-6}$ at RT, $\delta = 1320 \times 10^{-6}$ at 770 °C, and $\delta = 1350 \times 10^{-6}$ at 960 °C. The Knight shift was due to the conduction electrons in metals. They introduced an “extra” effective field at the nuclear site, due to the spin orientations of the conduction electrons in the presence of an external field. Depending on the electronic structure, the Knight shift may be temperature dependent. However, in metals which normally have a broad featureless electronic density of states, Knight shifts are temperature independent. It means that the detection of a particularly strong temperature dependency of the Knight shift indicates a formation of an electronically conductive phase in the system. The position of our “solid” line ($\delta = 1338 \times 10^{-6}$) is, as already stated, very close to that observed by Bastow et al. [20], and this signal can be attributed to an electronically conductive solid Sc–Al alloy formation. The finding is also the confirmation of the reaction in our system $(\text{NaF}-\text{ScF}_3)_{\text{eut}}-\text{Al}$ between the aluminum metal and the melt.

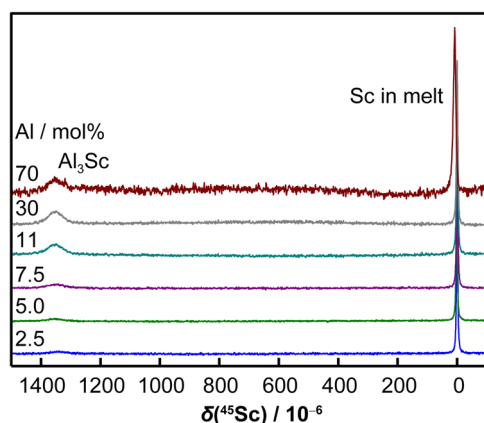


Fig. 6 ^{45}Sc HT NMR spectra of $(\text{NaF}-\text{ScF}_3)_{\text{eut}}-\text{Al}$ melts at 770 °C as a function of Al concentration

No changes in ^{45}Sc HT NMR spectra with time were observed within 5 min of experimental stabilization, suggesting the fast establishing of the equilibrium in the reaction mixture.

In case of the HT ^{27}Al NMR spectra of the samples with higher concentration of Al (60 mol%, Fig. S3), two resonance lines like in case of ^{45}Sc were also expected to be observed. However, both detected lines are narrow in this case, indicating on the first sight the only presence of the liquid state; one in the range, another one at around 1605×10^{-6} . In this case, any broader line could not identify the presence of the solid phase. However, it might be worth to note that, at high temperatures, Bastow et al. [20] observed a ^{27}Al line broadening with such a large extent that the authors were even not able to measure the line’s width. This observation in this work was explained by “the constitutional vacancies associated with the non-stoichiometry assist Al diffusion at anomalously low temperatures relative to the melting point”.

A small drift (from 23 to 30×10^{-6}) of the line attributed to AlF_5^{2-} species can be also seen with the increasing of the aluminum (Fig. S3). The evolution of the chemical shift indicates an increase of tetrahedral environments of Al. The similar behavior was also observed for the molten system $\text{NaF}-\text{AlF}_3$ [23, 26, 27]: $\delta(^{27}\text{Al}) \approx 14 \times 10^{-6}$ at 20 mol% AlF_3 and $\delta(^{27}\text{Al}) \approx 27 \times 10^{-6}$ at 35–40 mol% AlF_3 .

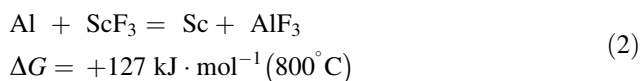
Also, a new signal (ca 1625×10^{-6}) in the mixture with the higher content of aluminum was detected, which is based on the results of the work [23] to the pure aluminum metal.

The experimental results demonstrate that the ^{19}F chemical shift is almost constant up to 20 mol% of Al (around -80×10^{-6}), and then it decreases from -80.5×10^{-6} to -148.6×10^{-6} with increasing concentration of Al metal. This change can be explained by the formation of Al–F linkages for high amount of Al, and consequently, an increase of the concentration of aluminum in the melt.

High-temperature ^{23}Na measurements were also taken in molten $(\text{NaF}-\text{ScF}_3)_{\text{eut}}-\text{Al}$ as a function of the different concentrations of aluminum. A decrease of the chemical shift values could be observed over the whole range of Al content. This reduction with Al addition corresponds to the increased shielding of the alkali cations. Therefore, the electronic cloud around the Na nucleus becomes more symmetric. This means that the Na–F interaction decreases with Al amount and sodium becomes more free.

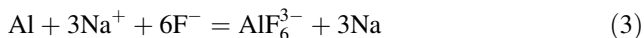
Interpretation of experimental results

Scandium can be difficult to be produced by the following reaction, since ΔG of the following reaction is positive:



However, the addition of aluminum to the molten NaF–ScF₃ eutectic mixture can really lead to the formation of a solid Al₃Sc alloy, as can be seen in previous paragraphs.

When some amount of aluminum was added into the eutectic NaF–ScF₃ melt (50 °C above the melting point), besides the formation of Al₃Sc, a small part of the aluminum metal gets dissolved into the melt which subsequently leads to the formation of Na₃AlF₆:



Since the Al₃Sc alloy is forming and precipitating from the liquid melt, the precipitation then leads to a change in the composition of the melt mixture. By this way, the amount of Sc in the melt is continually decreasing with increasing amount of Al₃Sc alloy precipitated off the melt. As the composition of the originally eutectic mixture (63 mol% NaF/ 37 mol% ScF₃) is being continually changed according to phase diagram, a formation of NaScF₄ and Na₃ScF₆ can be seen [10]. That was the reason why the presence of NaScF₄ and Na₃(Al,Sc)F₆ has been detected in XRD patterns of the solidified samples with low addition of aluminum. When the amount of ScF₃ in the melt dropped below 25 mol%, only Na₃(Al,Sc)F₆ was formed.

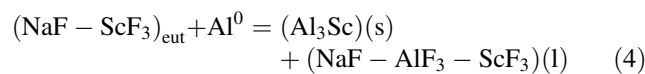
When more than 40 mol% of aluminum was added to the molten NaF–ScF₃ eutectic mixture, all amount of the scandium in the original melt would be consumed in the formation of Al₃Sc. This corresponds with our findings of the presence of Al₃Sc and the presence of unreacted part of aluminum and Na₃AlF₆ in the solidified samples with the very high addition of aluminum. However, it should be noted that some small traces of NaScF₄ and Na₃(Al,Sc)F₆ compounds were also found (MAS NMR and XRD) in the solidified samples containing 50 mol% of aluminum. A back reaction(s) during the natural cooling of the samples could be an explanation of the finding of these traces of scandium species.

Molecular dynamics modeling with density functional theory approach

To have a better understanding of reaction mechanism in our process, molecular dynamics simulations (MDs) and density functional theory (DFT) calculations were postulated to match the HT NMR experimental results. This methodology was already proven as a success in different molten fluoride systems: NaF/KF–AlF₃ [9, 28], NaF–AlF₃–Al₂O₃ [29], NaF–ScF₃ [7], LiF/NaF/KF–ZrF₄ [30] and LiF–ThF₄–UF₄ [31]. Molecular dynamics modeling with

density functional theory approach can be used to determine the speciation of the melt and to help to predict its physico-chemical behavior (density, electrical conductivity, viscosity, etc.).

When aluminum is added into the molten eutectic mixture of NaF–ScF₃, some part of the aluminum reacts to form an Al₃Sc solid alloy, and the remaining melt is basically the NaF–AlF₃–ScF₃ system. The whole process can be described by the following reaction:



The melt contains the fluoroscandate, fluoroaluminate species and very likely the fluoroalumosandate complexes. The high-temperature liquid, which is essentially reaction mixture where the formation and the precipitation of Al₃Sc solid alloy takes place, therefore contains four ions: Na⁺, Al³⁺, F[−] and Sc³⁺. In order to find out a qualitative/quantitative composition and the chemistry of this liquid reaction mixture, a further calculation and an additional HT NMR analysis of the specific NaF–AlF₃–ScF₃ system have been then carried out.

By balancing the total electrical charge to zero in order to ensure the electro-neutrality of the system, the compositions of this molten mixture were calculated from initial number of Sc (N_{Sc}) atoms, the initial number of aluminum atoms introduced (N_{Al}) and the amount of x Al₃Sc atoms formed during Reaction (4). To proceed with further calculations, and to find the correct mixture's compositions, a model was used based on the NaF–ScF₃–AlF₃ mixture with the different compositions presented in Table S1. The model is based on the fact that as more aluminum is added to the reaction mixture, the more the Al₃Sc solid alloy is being precipitated. The composition of NaF–ScF₃–AlF₃ molten system is then changing with concentration of AlF₃. The model is thus based on the direct linear relationship between the production of Al₃Sc and the gradual change in the composition of the molten part of the reaction mixture (NaF–ScF₃–AlF₃). From the results presented in Table S2, one can also see the efficiency of the process (ratio $N_{\text{Al}_3\text{Sc}}/N_{\text{Al}}$) of the formation of Al₃Sc (770 °C). The different compositions of the molten NaF–ScF₃–AlF₃ system (calculated based on the above-mentioned model) were then used in subsequent experimental HT NMR analysis, as well as in the related molecular dynamic simulations.

Figure 7a displays the ²⁷Al and ⁴⁵Sc NMR results in samples in which aluminum powder (15 μm grain) was added directly in NaF–ScF₃ (60 mol%–40 mol%) and ternary NaF–ScF₃–AlF₃ mixtures. Observation of good overall agreement between two systems confirmed the reaction mechanism 4 and allows us to start MD and DFT calculations. Figure 7b shows the HT NMR experimental

data of molten NaF–ScF₃–AlF₃ in comparison with the data calculated based on the molecular dynamic simulations. The chemical shift is one of the most sensitive indicators of the local structure, particularly for the first neighbors, i.e., for the coordination numbers and the corresponding bond lengths. A good agreement between the experimental values and the calculated values of the chemical shift is observed. This agreement indicates that our modeled approximation of the studied system (with Al) by that of containing AlF₃ is correct, and that the ion model used in these simulations is capable to reproduce accurately the NMR data related to the local structure around each nucleus in the molten NaF–ScF₃–AlF₃ system.

The analysis of ionic trajectories from molecular dynamics calculations also allows us to study the anionic species formed in the melts as a function of the AlF₃ concentration. Figure S4 shows the evolution of the radial distribution functions as a concentration of AlF₃. Based on the statistical mechanic, the radial distribution function contains a pair of correlation functions, which describes how density varies as a function of distance from a particle. The results presented in Fig. S4 were calculated from the ion positions for the following ionic pairs: Al–Al, Sc–Al and Sc–Sc. As it can be seen, the presence of a double first peak was observed for each pair. These distribution functions also show a very pronounced minimum, located on average around 0.42, 0.44 and 0.46 nm for the pairs Al–Al, Al–Sc and Sc–Sc, respectively, which defines the first

coordination sphere around the related ions, Al³⁺ and Sc³⁺. The radial distribution function of Al–Al and Sc–Sc pairs also shows the appearance of a localized pre-pic at around 0.3 nm, whose amplitude increases with the increase of the AlF₃ concentration. According to previous studies performed on the other fluoride-containing systems [29, 32], this medium-distance order means that the Al–Al and Sc–Sc distances are shortened due to the presence of fluorine ions. The presence of fluorine ion tends to simply bridge the Al–Al and Sc–Sc ion pairs. The intensity of this phenomenon is a function of the AlF₃ concentration in the melt.

The qualitative analysis based on the radial distribution function is visualized in Fig. 8, where a snapshot, extracted during the molecular dynamics calculation performed on the NaF–ScF₃–AlF₃ molten mixture, is depicted (4 mol% of AlF₃). For a better observation, the sodium ions were deliberately omitted. The figure shows a presence of a several ionic species: free fluorine F[−] anions, complexes ScF₆^{3−} and more complex compounds such as dimers Sc₂F₁₁^{5−} and chains Sc₂AlF₁₃^{4−}. This chained Sc₂AlF₁₃^{4−} is an exact example of the Al–Al and Sc–Sc bringing fluorine ions mentioned above.

Using distances between Al–F and Sc–F atoms determined from the first minimums of the radial distribution functions, one can calculate the mean coordination numbers around the aluminum and scandium ions in the melt (770 °C). Figure 9 shows the evolution of the anionic

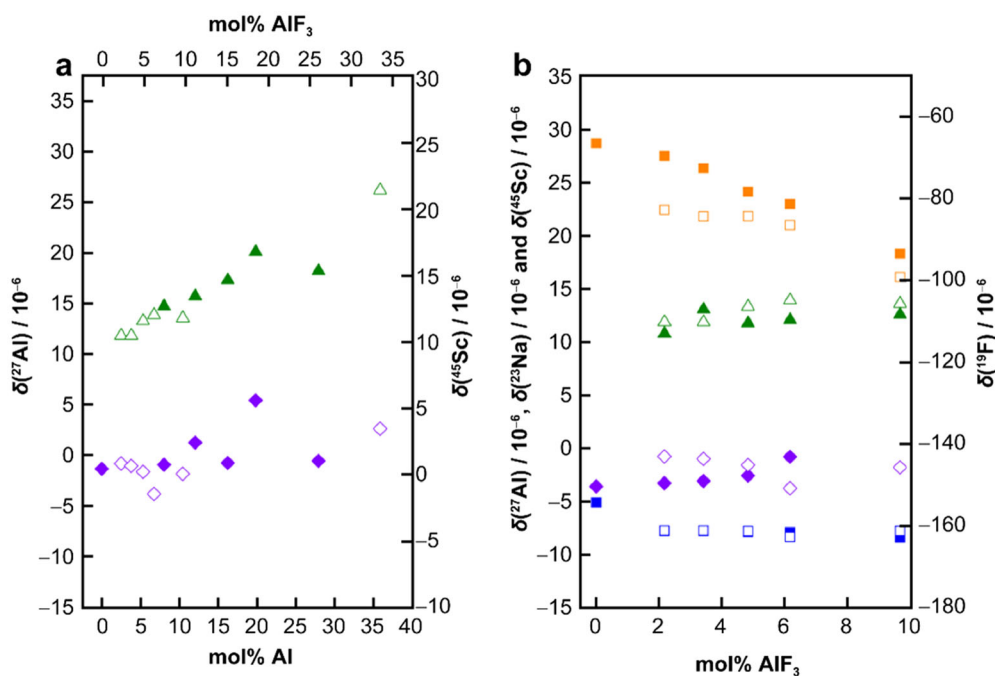


Fig. 7 NMR chemical shifts in liquid phases: **a** comparison of experimental data obtained for NaF–ScF₃–AlF₃ (empty symbols) and NaF–ScF₃–Al (solid symbols); **b** experimental (empty symbols) and calculated (solid symbols) data on molten mixture NaF–ScF₃–AlF₃ at 770 °C as a function of AlF₃ concentration

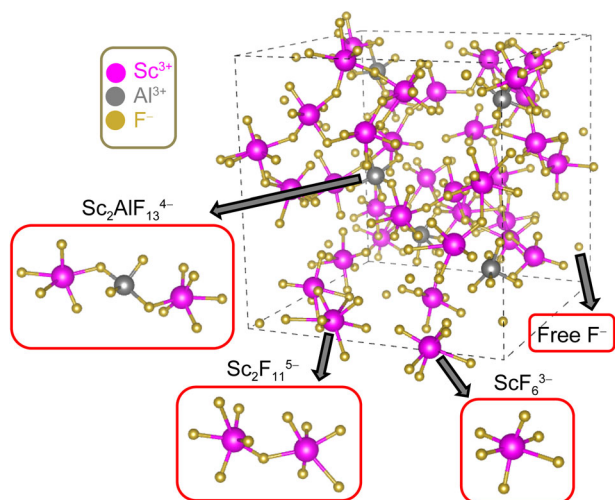


Fig. 8 Visualization of one snapshot from molecular dynamic trajectory for molten NaF–ScF₃–AlF₃ system with 4 mol% of AlF₃ sodium ions has been deliberately omitted for a better observation, where average lengths of Al–F and Sc–F bonds are 0.273 and 0.293 nm, respectively

complexes of aluminum and scandium, as a function of the molar concentration of AlF₃. Al³⁺ ions are mainly surrounded by 4, 5 or 6 neighboring F atoms, but the AlF₅²⁻ remains the most prevalent and the most stable species over the entire concentration range. This explains why the average number of aluminum coordination oscillates around an average value of 5. The value tends to decrease slightly with an increased concentration of AlF₃ in the original melt. This trend is due to a continual increase of the presence of the less coordinated AlF₄⁻ species with a concomitant decrease of the presence of the higher coordinated AlF₆³⁻ anions.

If considering Fig. 9 on the evolution of the coordination of scandium atoms as a function of the AlF₃ concentration in the melt, only two anionic complexes can be

seen: ScF₆³⁻ and ScF₅²⁻. The ScF₆³⁻ ion remains as the most prevalent species in the melt with lower concentrations of AlF₃ (up to ca 15 mol%), since at the higher concentrations of AlF₃ the most prevalent species becomes ScF₅²⁻. This inverse change in the species prevalence explains the gradual decrease of the average coordination number of scandium from 5.7 to 5.4 as the AlF₃ concentration increases.

The numerical results about the coordination of aluminum and scandium atoms in molten state suggest that the proposed model of the calculations in this case agrees well with our experimental HT NMR observations. At this point, we would like to again mention that as seen in Fig. S5, the majority of the scandium complexes are based on our calculations probably in real melt connected together via fluorine ions to form more or less long chains.

A detailed statistical analysis of the different atomic configurations recorded over a molecular dynamic range of 5 ns is shown in Fig. S5. Different species have been grouped for greater clarity into 6 major families: F⁻ free ions, monomers AlF_x^{3-x} (x = 4, 5, 6) or ScF_y^{3-y} (y = 5, 6) and “polymer” chains of the type Sc_xF_y^{3x-y}, Al_xF_y^{3x-y}, Sc_xAl_yF_z^{3x+3y-z}. As it can be seen from the figure, Sc_xAl_yF_z^{3x+3y-z} is the most prevalent species over a wide range of the AlF₃ concentration in the melt. In the melt, the highest proportion of this species is with approximately 10 mol% of AlF₃, when it gradually decreasing and is being exceeded by Al_xF_y^{3x-y} chains and by AlF_x^{3-x} monomers at the higher AlF₃ content. These calculated results are in very good agreement with what was found as the presence of a solid solution of Na₃(Al,Sc)F₆ detected by XRD and MAS NMR in the solidified samples and discussed above.

As it can be also seen from Fig. S5, the presence of the free fluorine anions and the presence of the isolated ScF_y^{3-y} complexes initially increase with the increase of

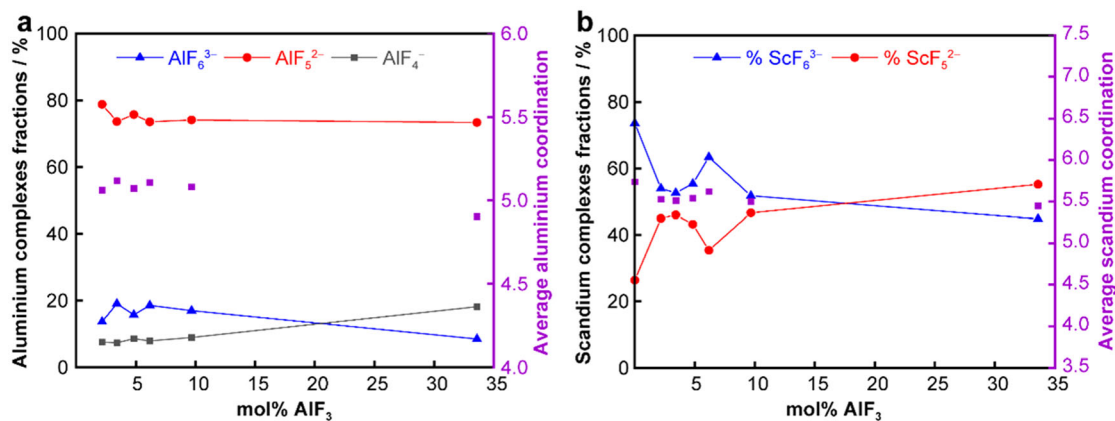


Fig. 9 a Aluminum and b scandium complexes fractions of AlF₅²⁻ (blue triangle), AlF₆³⁻ (red dot), AlF₄⁻ (black square), ScF₆³⁻ (blue triangle), ScF₅²⁻ (red dot), and average coordination (violet square) as a function of concentration of AlF₃ in molten NaF–ScF₃–AlF₃ system at 770 °C

the AlF_3 content before reaching a peak at 7.5 mol%. At the higher concentrations than 7.5 mol% of AlF_3 , a disappear of both species can be seen, too.

When considering the pure eutectic mixture of NaF-ScF_3 (absence of AlF_3), the mixture is essentially a network of $\text{Sc}_x\text{F}_y^{3x-y}$ chains in coexistence with some isolated complexes of ScF_y^{3-y} and free fluorine ions. These findings are in good agreement with what was already reported in Ref.[7]. The addition of aluminum into the molten NaF-ScF_3 system breaks right away the Sc-F bonds of $\text{Sc}_x\text{F}_y^{3x-y}$ networks and makes them possible to form isolated AlF_x^{3-x} complexes with subsequent release of more free fluorine ions. The introduction of aluminum atoms into the NaF-ScF_3 melt is thus responsible for the slight increase of free fluorine ions as also seen in Fig. S5.

As the amount of AlF_3 in the melt increases, the previously isolated complexes of AlF_x^{3-x} start to connect the chains of $\text{Sc}_x\text{F}_y^{3x-y}$ and form more complex network of chains of $\text{Sc}_x\text{Al}_y\text{F}_z^{3x+3y-z}$. As the concentration of AlF_3 increases more, the isolated complexes of AlF_x^{3-x} also start to connect together and form $\text{Al}_x\text{F}_y^{3x-y}$ chains. At the end, in the real melt, we can thus see the coexistence of two networks of $\text{Sc}_x\text{Al}_y\text{F}_z^{3x+3y-z}$ and $\text{Al}_x\text{F}_y^{3x-y}$ with some isolated complexes of AlF_x^{3-x} . The rearrangement of the network structure in the liquid phase must have also correlated with a change of the physico-chemical behavior of the melt like it can be really seen in Fig. 10 where values of density calculated based on the MD simulations as a function of the AlF_3 concentration are depicted. In the figure, the change in slope of the density can be seen somewhere between the concentration 5 mol% and 10 mol% of AlF_3 .

Going further in the considerations of the structure and the physico-chemical behavior of the melt, the dynamics of exchanges between Al^{3+} , Sc^{3+} and F^- ions was used to evaluate the lifetime of the anionic complexes formed in this molten system. The relaxation time of the first

coordination spheres of the Al^{3+} and Sc^{3+} ions as a function of the $\text{NaF-ScF}_3\text{-AlF}_3$ composition at 770 °C is already reported in Fig. S6. These relaxation time was determined by positioning themselves at the value of $1/e$ of the cage autocorrelation functions calculated according to the method of Rabani et al. [33]. These functions represent the time taken by a fluorine ion to leave the coordination sphere of the Al^{3+} or Sc^{3+} ions (Fig. S6). The calculations show that the average residence time of a fluorine ion around an Al^{3+} ion (about 20 ps) is four times longer than that of a fluorine ion around a Sc^{3+} ion (about 5 ps). However, this difference is being reduced as AlF_3 content in the melt increases.

The barrier energy based on the calculation of the potential of mean force (PMF) [34] of the ionic pairs $\text{Al}^{3+}\text{-F}^-$ and $\text{Sc}^{3+}\text{-F}^-$ (Fig. S7) was also calculated using the radial distribution function. This barrier energy corresponds to the energy difference between the first maximum and the first minimum of PMF $\psi(r) = -k_B \cdot T \cdot \ln g(r)$, where k_B is Boltzmann's constant and $g(r)$ is the radial function distribution function for a given pair of ions. As it can be seen in Fig. S5, the barrier energy of the ionic pair $\text{Al}^{3+}\text{-F}^-$ was found to be higher than that of the $\text{Sc}^{3+}\text{-F}^-$ pair.

This finding indicates that the fluorine ions contained in the aluminum coordination sphere are more difficult to separate off than those of the F^- ions located in the scandium environment. The instability of the scandium F^- -local environment compared to the aluminum one is probably responsible for the numerous exchanges of fluorinated neighbors in the vicinity of the scandium ions, and this fact can be also an explanation for the existence of the polymerization interactions in this molten system and thus formation of different complex chains (e.g., $\text{Sc}_x\text{F}_y^{3x-y}$, $\text{Al}_x\text{F}_y^{3x-y}$, $\text{Sc}_x\text{Al}_y\text{F}_z^{3x+3y-z}$).

It was already stated above that the combination of the theoretical approach proposed in this work can be used for the calculation of the physico-chemical behavior of the

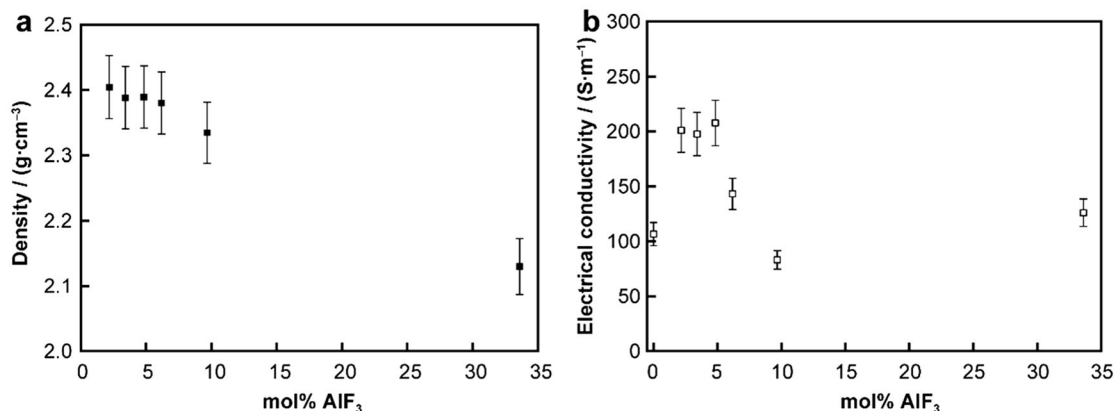


Fig. 10 a Density and b ionic electrical conductivity of molten $\text{NaF-ScF}_3\text{-AlF}_3$ system based on MD simulations (770 °C)

melt. The density of the molten NaF–ScF₃–AlF₃ system calculated based on the MD simulation at 770 °C is yet mentioned in Fig. 11. The similar evaluation of the transport properties of the molten NaF–ScF₃–AlF₃ system is presented in the following paragraphs.

An ionic electrical conductivity of the molten NaF–ScF₃–AlF₃ system calculated based on the MD simulations (770 °C) is depicted in Fig. 10. The electrical conductivity was calculated using a mean square displacement (MSD) of the atoms when the MS dynamics simulation of 5 ns was applied. The details of the approach used here are more described in our previous works [7, 9].

As it can be seen in Fig. 10, the electrical conductivity of the NaF–ScF₃ melt increases at the beginning sharply with the introduction of AlF₃ to the melt. This trend has a peak around 5 mol% of AlF₃ (200 S·m⁻¹), and then a sharp decrease of the conductivity can be seen reaching a conductivity of 75 S·m⁻¹ at 10 mol% of AlF₃. The conductivity goes afterward through a local minimum at approximately 15 mol% with a subsequent slow increasing toward higher concentrations of AlF₃ in the melt.

It can be noticed that the shape of the evolution of the conductivity for the concentrations below 30 mol% of AlF₃ resembles the shape of the evolution of the proportion of the presence of ScF_y^{3-y} species in the melt (see Fig. 10). The slow increase of the conductivity at the higher concentrations seems to be on the other hand more related with the increased presence of the AlF_y^{3-y} species in the melt or, simply, with the combination of different trends linked with the rearrangement of the internal environment of the melt as it was already discussed above.

The self-diffusion coefficients of the particles in the melt can be calculated in absence of external electric fields

using a slope of the function between MSD of the individual particles and time. MSD is based on the statistical mechanics to measuring of the deviation of the position of a particle subjected to a Brownian motion with respect to a reference position over time. The correction proposed by Yeh and Hummer [35] was also introduced in our approach to correct the effect of periodic boundary conditions. The self-diffusion coefficients calculated for each ion along the isotherm at 770 °C are presented in Fig. 11 as a function of the composition of the melt. Figure 11 also contains an inserted figure depicting the total diffusion coefficient as a result of the collective effects between the particular ions.

As it can be seen in Fig. 11, the sodium ions are the fastest diffusing ions regardless of the composition of the melt. The figure also shows that diffusion rate of F⁻, Al³⁺ and Sc³⁺ ions reaches the approximately same rate, at the higher concentrations of AlF₃. However, this rate is still 3.5 times slower than that of sodium ions. These observations are in good agreement with our structural analysis where it has been showed that all the fluorine ions are involved in the complexification interactions in the melt. It can be stated that regardless of the composition, there is probably no free F⁻ in our melt.

In terms of the viscosity as the other transport property of our system, the Green–Kubo formalism [36] was used for its prediction where a time integral of the autocorrelation function obtained by molecular dynamics over a 5-ns long trajectory was applied. The results of that calculation as a function of the AlF₃ concentration are depicted in Fig. 11. As it can be seen in the figure, the viscosity sharply drops upon the introduction of AlF₃ in to the system. After this sharp drop, the evolution of the viscosity with the increasing concentration of AlF₃ then shows a local

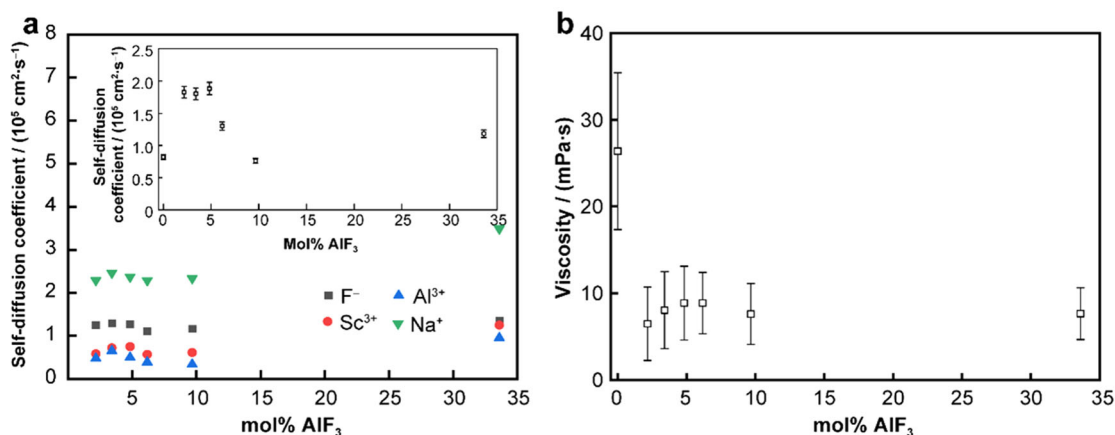


Fig. 11 **a** Self-diffusion coefficients of sodium (green nabla), aluminum (blue triangle), scandium (red dot) and fluorine ions (black square) obtained from molecular dynamic simulations in NaF–ScF₃–AlF₃ system at 770 °C, and (insert) total self-diffusion coefficients from these diffusion coefficients taking into account collective effects between ions; **b** calculated values of viscosity of molten NaF–ScF₃–AlF₃ mixtures as a function of AlF₃ concentration (770 °C), where Green–Kubo formalism [36] was used based on a time integral of autocorrelation function (5 ns)

maximum at around 5 mol% of AlF_3 and then a relative constant value in the range between 10 mol% and 35 mol% of AlF_3 .

The initial relatively sharp drop of the viscosity can be explained by the breakage of the original highly viscous network of the $\text{Sc}_x\text{F}_y^{3x-y}$ chains when AlF_3 is introduced into the melt. Another peak of the viscosity, calculated at the concentration around 5 mol%, can be then explained by a formation of the $\text{Sc}_x\text{Al}_y\text{F}_z^{3x+3y-z}$ species in the melt. Afterward, the viscosity slightly decreases toward a relatively constant value, probably due to a formation of a network of the $\text{Al}_x\text{F}_y^{3x-y}$ species which partially compensates the decrease in the presence of the $\text{Sc}_x\text{Al}_y\text{F}_z^{3x+3y-z}$ chains as can be seen in Fig. S5. It can be generally stated here that even in the case of the viscosity, the general behavior is in good agreement with our structural considerations. At the beginning, a sharp change of the physico-chemical behavior related to the breakage of the original the $\text{Sc}_x\text{F}_y^{3x-y}$ network can be seen. The further increase of the concentration of AlF_3 leads generally to the smaller changes in the melt behavior. It can be caused by the rearrangement of the internal environment of the melt related to the gradual change of the proportion of each species in the melt.

Conclusion

A combination of thermal analysis, in situ HT-NMR, solid-state NMR, powder XRD and molecular dynamics simulations gives first insight into the structure of molten NaF-ScF_3 eutectic with Al metal mixtures. By means of thermogravimetry method, the stability of the system was carried out in the molten state. The solubility of aluminum in the eutectic system of NaF-ScF_3 was analyzed by thermal analysis. During the in situ studies, ^{19}F , ^{23}Na , ^{27}Al and ^{45}Sc chemical shift evolutions prove the formation of an insoluble Al_3Sc alloy in molten bath. It should be noted that this reaction is very fast. In addition to the precipitation of Al_3Sc , the melt contains a small part of the soluble aluminum metal. Corresponding ex situ examinations bring to light the formation of NaScF_4 and solid solution of $\text{Na}_3(\text{Al}, \text{Sc})\text{F}_6$ in cooled bath.

Based on the validity of the polarizable ion model and a good agreement between the experimental values and the calculated values of the chemical shift, the local structure in molten salt was reported. Additionally reliable physico-chemical properties of the molten bath (density, electrical conductivity, self-diffusion coefficients, viscosity) were predicted.

This work represents the first step in systematic effort aiming at the elucidation of the role of structure and composition of melts in the Al-Sc alloy production process and provides new perspectives for the optimization,

simplification and cost reduction of the manufacturing of aluminum-scandium alloy.

Acknowledgements For DFT calculations, we thank the “Centre de Calcul Scientifique en region Centre” (Orleans, France). Financial supports from the IR INFRANALYTICS FR2054, from Slovak grant agency (VEGA 2/0046/22), and ITMS project (with code 313021T081) supported by Research and Innovation Operational program funded by the ERDF, for conducting the research are gratefully acknowledged. AD acknowledges the Kazan Federal University Strategic Academic Leadership Program» (Priority-2030). The authors also thank to Dr. F. Vivet for fruitful discussions.

Funding Open access funding provided by The Ministry of Education, Science, Research and Sport of the Slovak Republic in cooperation with Centre for Scientific and Technical Information of the Slovak Republic.

Declarations

Conflict of interests The authors declare that they have no conflict of interest.

Open Access This article is licensed under a Creative Commons Attribution 4.0 International License, which permits use, sharing, adaptation, distribution and reproduction in any medium or format, as long as you give appropriate credit to the original author(s) and the source, provide a link to the Creative Commons licence, and indicate if changes were made. The images or other third party material in this article are included in the article’s Creative Commons licence, unless indicated otherwise in a credit line to the material. If material is not included in the article’s Creative Commons licence and your intended use is not permitted by statutory regulation or exceeds the permitted use, you will need to obtain permission directly from the copyright holder. To view a copy of this licence, visit <http://creativecommons.org/licenses/by/4.0/>.

References

- [1] Fujikawa SI, Sugaya M, Takei Hajime, Hirano KI. Solid solubility and residual resistivity of scandium in aluminum. *J Less-common Met.* 1979;63:87. [https://doi.org/10.1016/0022-5088\(79\)90211-X](https://doi.org/10.1016/0022-5088(79)90211-X).
- [2] Kaya Ş, Dittrich C, Stopic S, Friedrich B. Concentration and separation of scandium from Ni laterite ore processing streams. *Metals.* 2017;7:557. <https://doi.org/10.3390/met7120557>.
- [3] Naboychenko SS, Murashova IB, Neikov OD. Handbook of Non-Ferrous Metal Powders. Oxford: Elsevier; 2005:485. <https://doi.org/10.1016/B978-1-85617-422-0.00022-7>.
- [4] Wang W, Pranolo Y, Cheng CY. Metallurgical processes for scandium recovery from various resources: a review. *Hydrometallurgy.* 2011;108:100. <https://doi.org/10.1016/j.hydromet.2011.03.001>.
- [5] Smyshlyaev VY. By-producing scandium from pregnant solutions during in-situ leaching at Dalmatovskoe uranium deposit. *Gorn Zhurnal.* 2017;8:28. <https://doi.org/10.17580/gzh.2017.08.05>.
- [6] Rychkov VN, Kirillov EV, Kirillov SV, Bunkov GM, Botalov MS, Poponin NA, Smirnov AL, Mashkovtsev MA, Smyshlyaev DV. Method of reprocessing of wasted scandium-containing solutions from uranium extraction. Russian Federation Patent 2016; 2622201.
- [7] Rakhmatullin A, Machado K, Zanghi D, Polovov IB, Bakirov R, Maksimtsev KV, Bessada C. Study of the NaF-ScF_3 system as a molten bath for production of Sc alloys: a combination of

- NMR and molecular dynamics simulations. *J Alloys Compd.* 2019;786:953. <https://doi.org/10.1016/j.jallcom.2019.02.057>.
- [8] Weingarth M, Bodenhausen G, Tekely P. Probing the quenching of rotary resonance by PISSARRO decoupling. *Chem Phys Lett.* 2011;502:259. <https://doi.org/10.1016/j.cplett.2010.12.040>.
- [9] Machado K, Zanghi D, Sarou-Kanian V, Cadars S, Burbano M, Salanne M, Bessada C. Study of NaF–AlF₃ melts by coupling molecular dynamics, density functional theory, and NMR measurements. *J Phys Chem C.* 2017;121:10289. <https://doi.org/10.1021/acs.jpcc.7b01530>.
- [10] Thoma RE, Karraker RH. The sodium fluoride-scandium trifluoride system. *Inorg Chem.* 1966;5:1933. <https://doi.org/10.1021/ic50045a021>.
- [11] Hyland RW. Homogeneous nucleation kinetics of Al₃Sc in a dilute Al–Sc alloy. *Metall Trans A.* 1992;23:1947. <https://doi.org/10.1007/BF02647542>.
- [12] Murray JL. The Al–Sc (aluminum-scandium) system. *J Ph Equilibria.* 1998;19:380. <https://doi.org/10.1361/105497198770342120>.
- [13] Bohnsack A, Meyer G. Ternäre halogenide vom typ A₃MX₆. IV. [1]. ternäre halogenide des scandiums mit natrium, Na₃ScX₆ (X = F, Cl, Br): synthese, strukturen, ionenleitfähigkeit. *Z Anorg Allg Chem.* 1996;622:173. <https://doi.org/10.1002/zaac.19966220125>.
- [14] Rechkin VN, Lamikhov LK, Samsonova TI. Crystal structures of some scandium aluminides. *Sov Phys Crystallogr.* 1964;9:325.
- [15] Holmberg B. The crystal structure of ScOF. *Acta Chem Scand.* 1966;20:1082.
- [16] Hawthorne FC, Ferguson RB. Refinement of the crystal structure of cryolite. *Can Mineral.* 1975;13:377.
- [17] Løusch R, Hebecker C, Ranft Z. Röntgenographische untersuchungen an neuen ternären fluoriden vom Typ TIII MF₆ (M = Ga, In, Sc) sowie an Einkristallen von ScF₃. *Z Anorg Allg Chem.* 1982;491:199. <https://doi.org/10.1002/zaac.19824910125>.
- [18] Swanson HE, Tatge E. Standard X-ray diffraction powder patterns, vol. 1. Gaithersburg: U.S. Department of Commerce, National Bureau of Standards; 1953.11.
- [19] Bräuniger T, Hofmann AJ, Moudrakovski IL, Hoch C, Schnick W. A ⁴⁵Sc-NMR and DFT calculation study of crystalline scandium compounds. *Solid State Sci.* 2016;51:1. <https://doi.org/10.1016/j.solidstatesciences.2015.11.002>.
- [20] Bastow TJ, Forwood CT, Gibson MA, Smith ME. Local site symmetry and electronic structure of trialuminide and related intermetallic alloys probed by solid-state NMR. *Phys Rev B.* 1998;58:2988. <https://doi.org/10.1103/PhysRevB.58.2988>.
- [21] Røyset J, Ryum N. Scandium in aluminium alloys. *Int Mater Rev.* 2005;50:19. <https://doi.org/10.1179/174328005X14311>.
- [22] Bono D, Hartig J, Huber M, Schnöckel H, de Jongh LJ. ²⁷Al NMR study of the metal cluster compound Al₅₀C₁₂₀H₁₈₀. *J Cluster Sci.* 2007;18:319. <https://doi.org/10.1007/s10876-007-0111-3>.
- [23] Nuta I, Veron E, Matzen G, Bessada C. High temperature NMR study of aluminum metal influence on speciation in molten NaF–AlF₃ fluorides. *Inorg Chem.* 2011;50:3304. <https://doi.org/10.1021/ic1019845>.
- [24] Rakhmatullin A, Polovov IB, Maltsev D, Allix M, Volkovich V, Chukin AV, Boča M, Bessada C. Combined approach for the structural characterization of alkali fluoroscandates: solid-state NMR, powder X-ray diffraction, and density functional theory calculations. *Inorg Chem.* 2018;57:1184. <https://doi.org/10.1021/acs.inorgchem.7b02617>.
- [25] Rakhmatullin A, Allix M, Polovov IB, Maltsev D, Chukin AV, Bakirov R, Bessada C. Combining solid state NMR, powder X-ray diffraction, and DFT calculations for CsSc₃F₁₀ structure determination. *J Alloys Compd.* 2019;787:1349. <https://doi.org/10.1016/j.jallcom.2019.01.355>.
- [26] Lacassagne V, Bessada C, Florian P, Bouvet S, Ollivier B, Coutures JP, Massiot D. Structure of high-temperature NaF–AlF₃–Al₂O₃ melts: a multinuclear NMR study. *J Phys Chem B.* 2002;106:1862. <https://doi.org/10.1021/jp0131141>.
- [27] Robert E, Lacassagne V, Bessada C, Massiot D, Gilbert B, Coutures JP. Study of NaF–AlF₃ melts by high-temperature ²⁷Al NMR spectroscopy: comparison with results from Raman spectroscopy. *Inorg Chem.* 1999;38:214. <https://doi.org/10.1021/ic980677b>.
- [28] Machado K, Zanghi D, Salanne M, Bessada C. Structural, dynamic, and thermodynamic study of KF–AlF₃ melts by combining high-temperature NMR and molecular dynamics simulations. *J Phys Chem C.* 2019;123:2147. <https://doi.org/10.1021/acs.jpcc.8b11907>.
- [29] Machado K, Zanghi D, Salanne M, Stabrowski V, Bessada C. Anionic structure in molten cryolite–alumina systems. *J Phys Chem C.* 2018;122:21807. <https://doi.org/10.1021/acs.jpcc.8b06905>.
- [30] Pauvert O, Salanne M, Zanghi D, Simon C, Reguer S, Thiaudière D, Okamoto Y, Matsuura H, Bessada C. Ion specific effects on the structure of molten AF–ZrF₄ systems (A⁺ = Li⁺, Na⁺, and K⁺). *J Phys Chem B.* 2011;115:9160. <https://doi.org/10.1021/jp203137h>.
- [31] Bessada C, Zanghi D, Salanne M, Gil-Martin A, Gibilaro M, Chamelot P, Massot L, Nezu A, Matsuura H. Investigation of ionic local structure in molten salt fast reactor LiF–ThF₄–UF₄ fuel by EXAFS experiments and molecular dynamics simulations. *J Mol Liq.* 2020;307:112927. <https://doi.org/10.1016/j.molliq.2020.112927>.
- [32] Pauvert O, Zanghi D, Salanne M, Simon C, Rakhmatullin A, Matsuura H, Okamoto Y, Vivet F, Bessada C. In situ experimental evidence for a nonmonotonous structural evolution with composition in the molten LiF–ZrF₄ system. *J Phys Chem B.* 2010;114:6472. <https://doi.org/10.1021/jp912195j>.
- [33] Rabani E, Gezelter JD, Berne BJ. Calculating the hopping rate for self-diffusion on rough potential energy surfaces: cage correlations. *J Chem Phys.* 1997;107:6867. <https://doi.org/10.1063/1.474927>.
- [34] Hansen JP, McDonald IR. *Theory of Simple Liquids.* 3rd ed. Burlington: Academic Press; 2006.78. <https://doi.org/10.1016/B978-012370535-8/50006-9>.
- [35] Yeh IC, Hummer G. System-size dependence of diffusion coefficients and viscosities from molecular dynamics simulations with periodic boundary conditions. *J Phys Chem B.* 2004;108:15873. <https://doi.org/10.1021/jp0477147>.
- [36] Ohtori N, Salanne M, Madden PA. Calculations of the thermal conductivities of ionic materials by simulation with polarizable interaction potentials. *J Chem Phys.* 2009;130:104507. <https://doi.org/10.1063/1.3086856>.

